Traveling wave model for laser-guided discharges

Martin Lampe,[a] Richard F. Fernsler, Steven P. Slinker,[a] and Daniel F. Gordon
Plasma Physics Division, Naval Research Laboratory, Washington, DC 20375, USA

(Received 4 June 2010; accepted 7 September 2010; published online 22 November 2010)

We present an easily solvable 1D traveling wave model for laser-guided discharges. By assuming constant propagation speed u, the hydro/electrodynamic/chemistry equations are reduced to ordinary differential equations in retarded time τ. Negative discharges are shown to propagate only if $u > \mu E_b$, where μ is electron mobility and E_b is the breakdown field; positive discharges propagate only if the channel preconductance exceeds $\sim 6 \times 10^{-11}$ m/Ω. The axial electric field E is shown to spike up to several times E_b and then relax to $\sim E_b$ for as long as the gas remains cold. In this streamer region, the channel conductance, current, and potential all increase linearly with τ. The transition to the leader stage, where E is much smaller, occurs in two steps: excitation of vibrational and low-lying electronic states, then gas heating. The propagation range decreases as a function of initial radius and (for given maximum voltage) of the voltage rise rate. Expansion of the hot channel is shown to increase the range. [doi:10.1063/1.3494160]

I. INTRODUCTION

There is an extensive literature[1–3] on the propagation of long filamentary discharges in gases, particularly air, and in recent years there have been a number of experimental studies of discharges guided over ranges of one to several meters, along conductivity channels created by ultrashort-pulse lasers.[4–17] Theoretical analyses are usually based on either 1D (axial) or 2D (r–z) simulation models. These types of models are particularly well suited to laser-guided discharges, which are constrained to follow the cylindrical conductivity channel laid down by the laser, as opposed to the meandering and often branched trajectory of unguided discharges, with multiple streamers typically coalescing at the head of the discharge. Laser-guided discharges are also simpler to understand in another way: at the onset of the electric discharge, there is already a substantial plasma density in the laser-prepared channel.[18–20,4] However, state of the art 2D models are severely limited by computational resources and as a result are typically run only to ranges ≤ 5 cm.[21–25] Even 1D models,[26–30] which often concentrate heavily on the air chemistry that ultimately determines the conductivity, are computationally intensive. A more fundamental issue is that the models can be so complicated that it is difficult to really understand the results, let alone extract the important physical features, scaling laws, and parametric dependences.

The purpose of this paper is to explore the consequences of a simpler type of model, initially introduced in Ref. 31, which is applicable to laser-guided discharges but not, in general, to discharges into ambient air. Our model is amenable to analysis and provides immediate insight into the structure and properties of the discharge; it can also be solved numerically, easily and quickly, over any range of interest. Like Wright,[32] Marode[33] and subsequent investigators, we use 1D transmission-line equations to model the discharge, but we make the additional key assumption that the discharge takes the form of a traveling ionization wave propagating at a *constant speed* u. This assumption allows us to reduce the problem to a set of ordinary differential equations in retarded time $\tau \equiv t - z/u$, which are amenable to analysis and immediate understanding. We show that the assumption of constant propagation speed is exactly correct for a particular form of the driving voltage pulse V(t), which we calculate in the analysis. More generally, we argue that in a real experiment where V(t) is the specified quantity, the propagation speed u(t) is typically a slowly varying function of time, and therefore the constant speed assumption, with u set equal to the instantaneous value of u(t), provides a quantitatively accurate model for the leading parts of the discharge and a qualitatively reasonable model for the entire discharge. We additionally assume that the discharge propagates within a well-defined channel previously laid down by a short-pulse laser, but we include hydrodynamic expansion of the channel as it is heated by the discharge. Air chemistry can be included at any desired level of detail; at present, the kinetics code CHMAIR-II[13,34] is used in the leading parts of the discharge, and we have the option to transition to a Saha model in the trailing parts where the air is hot and close to local thermodynamic equilibrium.

We should note at the outset some aspects of the problem that are not treated in this paper. Our intended focus is on the propagation of discharges, typically over distances >50 cm from a single electrode biased to >100 kV, after a streamer has formed and propagated away from the electrode along the laser channel, but before the discharge has connected to ground. Since it is not our intention to model the initial formation of the discharge at the electrode, we do not treat the low-voltage sheath which forms at the electrode, but instead assume that the electrode can absorb or supply electrons as needed by the discharge. We also make an important simplification in our modeling of the conductivity channel left behind by the laser. In air, electrons ionized by the laser attach to oxygen before the discharge arrives, leaving a substantial density of negative ions. However, these weakly bound electrons are easily and rapidly detached by visible or

[a]Retired.

Downloaded 10 Feb 2011 to 132.250.22.10. Redistribution subject to AIP license or copyright; see http://pop.aip.org/about/rights_and_permissions

even IR radiation at the discharge tip. We shall not study this part of the problem in the present paper, but rather represent the effect of the laser as leaving behind a specified channel electron density n_{e0} when the discharge arrives. We further assume that over the course of the discharge, photodetachment proceeds at a rate $\nu_a n_{e0}$, sufficient to maintain the initial electron density n_{e0} despite the losses to attachment at rate ν_a.

We are able to derive a number of remarkable conclusions, some new and some known experimentally but previously not well understood. The outline of the paper is as follows. In Sec. II we present the model and discuss its underlying assumptions. In Sec. III–V we consider the region at the front of the discharge where the degree of gas heating and excitation is low and the Townsend model (in which the electron-neutral collision rates are functions of the instantaneous electric field) is reasonably justified.[3] We refer to this as the "streamer" region. In the context of the present paper, there is no implication that streamers are multiple or branched; instead we show that a single laser-initiated streamer can grow into a "leader," which we define as the region of the discharge where the air is hot and highly excited. According to the 1D model, the structure of the discharge in the streamer region depends on only two parameters, the propagation speed u and the conductance Σ_0 of the laser channel. In Sec. IV we consider the streamer region of a negative discharge and prove that the propagation speed of a negative discharge must exceed μE_b, where μ is the electron mobility and $E_b \approx 2.7$ MV/m is the breakdown electric field for cold air at ambient density. At this point we show that the model is valid only when the initial conductance is sufficiently large and the initial channel radius sufficiently small. For these reasons, the model does not apply to discharges into ambient air, where the seed electrons are believed to be due to photoionization.[2] In Sec. V we consider the streamer region of a positive discharge, and prove that for successful propagation at velocity u, Σ_0 must exceed a threshold value that is $\sim 6\times 10^{-11}$ m/Ω for $u < 10^6$ m/s, but increases rapidly for larger u. For both positive and negative polarities, the axial electric field rapidly rises to a peak value (the "E-spike") several times the breakdown field E_b and then settles down to a value close to E_b, which persists until the gas becomes highly excited. This general behavior occurs whether or not electron-attaching species are present; in the presence of an attaching gas like oxygen, the electric field simply increases slightly, to the extent necessary for ionization to balance attachment. We show that the voltage, current, and conductivity are all still small at the E-spike and therefore (assuming the separate thresholds for positive and negative discharges are exceeded) this initial breakdown region has little influence on the structure and energetics of the rest of the discharge. In particular, after the E-spike the value of Σ_0 no longer plays any significant role and there is no qualitative difference between discharges of positive and negative polarities. Thus, in the streamer region behind the E-spike, the structure of the discharge depends on only a single parameter, the discharge propagation speed u. In this region, we find that the conductance $\Sigma(\tau)$, the current $I(\tau)$, and the potential $\phi(\tau)$ all increase nearly linearly with τ.

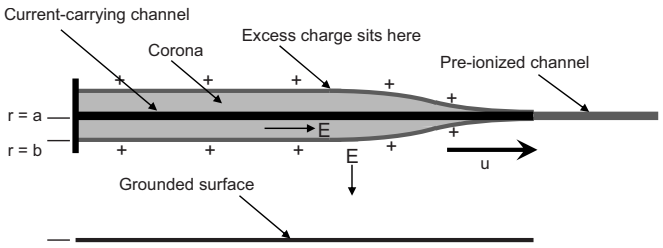

FIG. 1. Sketch showing the overall geometry of the discharge, following the traveling wave transmission-line model.

In Secs. VI and VII we consider the transition to the leader phase where the air is hot and excited. This transition occurs in two stages, first the vibrational and low-lying electronic states are excited, and later the gas is heated. As discussed in the previous paragraph, electron attachment is not a determining feature of the streamer region; thus we find (in contrast with the view put forth by Gallimberti)[1] that thermal detachment of attached electrons is not the triggering mechanism for the streamer/leader transition. We show that $E(\tau)$ is much smaller in the leader region, permitting propagation of the discharge to longer range. In this part of the discharge, we find that the initial discharge radius a_0 is a critical parameter since it determines the number of air molecules included in the discharge. The initial radius a_0 is determined by the radius of the laser filament and by recombination processes occurring within the laser channel. All other things being equal, the discharge range (for any given driving voltage) decreases strongly as a_0 increases, because the discharge energy is spread among more molecules. However, we find that radial expansion of the heated air, which increases the discharge volume without changing the number of molecules within the discharge, greatly increases the range, as previously discussed by Kulikovsky.[23] We also find that the propagation range of a discharge is a decreasing function of the voltage rise rate $\dot{V}(t)$ for a given maximum voltage V_{max}. Our conclusions are summarized in Sec. VIII

II. MODEL

Our work in this paper is based on a 1D transmission-line model of the discharge, as illustrated in Fig. 1. Transmission-line models have been used in many previous studies,[32,33] but for clarity we begin by listing the assumptions that are made in deriving a 1D transmission-line model from the full Maxwell's equations:

(1) The axial current flows within a radially uniform conducting channel of radius a(z,t), from an electrode located at z=0 toward the discharge tip located at z =L(t). The initial radius $a_0(z,t)$ is determined by the laser and recombination processes occurring within the laser channel. In this paper we do not calculate $a_0(z,t)$ self-consistently but simply specify it as an input, and in our examples we set $a_0(z,t)$ equal to a constant a_0, taken to be 200 μm in our baseline case. (Short-pulse lasers typically produce plasma filaments that are even narrower, but electron-ion recombination proceeds most rapidly on axis, thereby broadening the plasma profile.)

Downloaded 10 Feb 2011 to 132.250.22.10. Redistribution subject to AIP license or copyright; see http://pop.aip.org/about/rights_and_permissions

As we shall show, the properties of the streamer region at the front of the discharge do not depend on $a_0(z,t)$, so the magnitude of a_0 is largely irrelevant there. However the value of $a_0(z,t)$ plays a crucial role later in the discharge where the channel is hot and excited. We do include a self-consistent treatment of the hydrodynamic expansion of the hot channel, which turns out to be an important feature in that part of the discharge. However, as this is a 1D model, we do not attempt to model "thermal instabilities," i.e., changes in the radial profile of conductivity that are associated with nonuniform channel heating.[3]

(2) The highly conducting current-carrying channel of radius a(z,t) is surrounded by a corona of radius b(z,t), with much lower conductivity, created by electrostatic breakdown. We assume that the space charge carried by the discharge sits in a shell at $r=b(z,t)$ and that b(z,t) is the radius where the radial electric field E_r equals the breakdown field E_b. In the leader region b(z,t) can be tens of centimeters, much larger than a(z,t). But at the tip of the discharge there is very little charge, E_r is small, and $b(z,t) \approx a(z,t)$.

(3) The length scale for axial variations is long compared with b(z,t), i.e.,

$$b(z,t)\left|\frac{1}{f}\frac{\partial f}{\partial z}\right| \ll 1, \tag{1}$$

for any variable f(z,t). As a consequence, the electric field is purely radial for $r \geq b$ (leading to a capacitive contribution to the transmission-line equation), and purely axial and independent of r for $r \leq b$ (leading to a resistive contribution). Equation (1) is well satisfied in most of the discharge but is questionable at the tip, especially when the pre-existing conductivity in the laser channel is low, as discussed in Sec. IV

(4) The electron flow velocity is given by a simple Ohm's law, $v=-\mu E$, where μ is the electron mobility. A pressure gradient/diffusion term is sometimes included in Ohm's law, but this is normally a small correction, which we neglect. This assumption is not crucial and is made only for convenience. The electron mobility is given in general by $\mu=e/m_e\nu_m$, where –e is the charge, m_e is the mass, and ν_m is the total momentum-transfer collision frequency of the electrons. In CHMAIR-II the collision frequencies between electrons and the various neutral and ion species are computed in terms of the electron temperature T_e, and the frequencies are then summed to obtain ν_m. μ varies with time, but weakly compared to the variation in μE. Therefore for the simplified presentation of the streamer regime in Secs. III–V, we treat μ as a constant,[3] set to 0.06 $m^2\ V^{-1}\ s^{-1}$, based on the assumption that the air is still cold and at atmospheric density ($n_{g0}=2.5\times10^{25}\ m^{-3}$).

With these assumptions, Maxwell's equations reduce to the charge conservation relationship

$$\frac{\partial(C\phi)}{\partial t}+\frac{\partial(\Sigma E)}{\partial z}=0, \tag{2}$$

where E is the axial electric field, C is the capacitance per unit length, ϕ is the electrostatic potential, $\Sigma \equiv N_e e\mu$ is the conductance (inverse of the resistance per unit length), and N_e is the number of electrons per unit length. $C\phi$ is the distributed charge and ΣE is the axial current. For a discharge that propagates parallel to and a distance R above a ground plane, $C \equiv 2\pi\varepsilon_0/\ln[(2R-b)/b]$, where $\varepsilon_0 \equiv 8.85\times10^{-12}$ F/m. C thus varies to some extent with (z,t) through its logarithmic dependence on b(z,t), but in the simplified presentation of Secs. III–V we shall treat C in the streamer region as a constant, set equal to 6×10^{-12} F/m. In the numerical solutions of Sec. VII, both C and μ are calculated self-consistently as functions of (z,t). However, the rapid increase of N_e by orders of magnitude during breakdown is the most important process in discharges, and we concentrate the discussion in Secs. III–V on this.

For discharges which propagate at speeds $u \ll c$, inductive effects are negligible and

$$E=-\partial\phi/\partial z, \tag{3}$$

so that Eq. (2) becomes

$$\frac{\partial(C\phi)}{\partial t}=\frac{\partial}{\partial z}\Sigma\frac{\partial\phi}{\partial z}. \tag{4}$$

Since $\Sigma \equiv N_e e\mu$, Eqs. (3) and (4) must be supplemented by an equation for N_e, which takes the form

$$\frac{\partial N_e}{\partial t}=\frac{\partial(N_e\mu E)}{\partial z}+(\nu_i-\nu_a)N_e+\text{detachment}-\text{recombination}+\cdots, \tag{5}$$

where ν_i and ν_a are the electron ionization and attachment rates. Higher-order processes (detachment, recombination, associative ionization, etc.) are only noted symbolically.

Since Eq. (4) is a diffusion equation, it may seem surprising that there are solutions in the nature of traveling breakdown waves. These solutions occur because ν_i in Eq. (5) is an extremely nonlinear function of E, which triggers the breakdown process and completely changes the mathematical character of the equations. Since discharges typically have a fairly constant or slowly varying propagation speed $u(t) \equiv \dot{L}(t)$, the problem can be further simplified by assuming that u is constant. All quantities then depend on z and t only through the retarded time $\tau \equiv t-z/u$, which can be regarded as the time since the tip of the discharge passed location z. Note that this is a specification, not an approximation; if we find such a solution, it will be an exact solution of the equations. Equations (3)–(5) then reduce to ordinary differential equations (ODEs),

$$\frac{d(C\phi)}{d\tau}=\frac{1}{u}\frac{d(\Sigma E)}{d\tau}, \tag{6}$$

Downloaded 10 Feb 2011 to 132.250.22.10. Redistribution subject to AIP license or copyright; see http://pop.aip.org/about/rights_and_permissions

$$\frac{d}{d\tau}\left[\left(1+\frac{\mu E}{u}\right)\Sigma\right]=(\nu_i-\nu_a)\Sigma+\text{detachment}-\text{recombination}+\cdots, \tag{7}$$

$$E=\frac{1}{u}\frac{d\phi}{dt}. \tag{8}$$

Neglecting the small term $dC/d\tau$, Eqs. (6) and (8) give

$$\frac{d(\Sigma E)}{d\tau}=Cu^2E. \tag{9a}$$

Setting the current to $\Sigma E=I=uC\phi$, Eq. (9a) can also be written as

$$\frac{dI}{d\tau}=Cu^2E, \tag{9b}$$

$$\frac{1}{I}\frac{dI}{d\tau}=\frac{Cu^2}{\Sigma}, \tag{9c}$$

or

$$\frac{1}{E}\frac{dE}{d\tau}=\frac{Cu^2}{\Sigma}-\frac{1}{\Sigma}\frac{d\Sigma}{d\tau}. \tag{9d}$$

Equations (7) and (9), together with the rate equations, comprise a set of ordinary differential equations in τ that completely determine E, I, and Σ as functions of τ. We shall refer to this as the traveling wave model. The equations are to be integrated from $\tau=0$, the tip of the discharge where $z=L(t)$, back toward the source at $z=0$ where $\tau=t$. The initial condition for $\Sigma(\tau)$ is $\Sigma(0)=\Sigma_0$, the channel preconductance. The initial condition for $E(\tau)$ is $E(0)=E_0$, where E_0 is essentially just a marker for the beginning of the discharge. The magnitude of E_0 is arbitrary; it can be any small value satisfying $0<|E_b|\ll E_b$ and $|v|=\mu|E_0|\ll u$. However, the *sign* of E_0 is crucial in that it determines the polarity of the discharge.

Note that in the traveling wave formulation, the propagation speed u (constant) is an *input* to the calculation while the voltage V(t) applied at the electrode is an *output*, obtained by first solving Eqs. (7) and (9a) and then computing $V(t)=\phi(0,t)=\int_0^{L(t)}dzE(z,t)=u\int_0^t d\tau E(\tau)$. Thus we have turned the problem around from the usual formulation, in which V(t) is specified and u(t) is calculated, and we have furthermore restricted our consideration to those pulse shapes that lead to constant u. Not surprisingly, for these pulse shapes V(t) is monotonically increasing. If, in an actual experiment, the applied voltage V(t) is flat-topped, u(t) will slowly decrease. Our constant-u traveling wave model is then quantitatively accurate from the tip of the discharge ($\tau=0$) back to $\tau\approx\tau_u$, where τ_u is the time scale over which u may be regarded as essentially constant. Further back from the head of the discharge, there will be some averaging over the range of values of u(t) that have previously occurred, but this averaging should not change the qualitative features of the model.

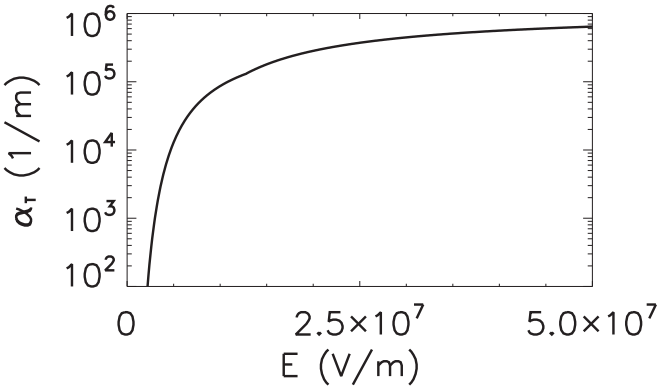

FIG. 2. Townsend coefficient α_T as a function of E in air at density $n_{g0}=2.5\times10^{25}$ m^{-3} from Eq. (11).

III. STREAMER REGION (COOL AIR)

In this section we begin to consider the leading part of the discharge where the degree of gas heating and excitation is weak. To facilitate understanding, we make some additional simplifications in modeling this region. First, we use the Townsend ionization model[3] (based on nearly a century of swarm data),[35] according to which the ionization rate ν_i depends only on the molecular number density n_g and the instantaneous electric field E, with ν_i/n_g a tabulated function of E/n_g. In this part of the discharge the gas is cold, thermal detachment is negligible, and n_g is constant; for specificity we set $n_g=n_{g0}=2.5\times10^{25}$ m^{-3}. Second, we treat the capacitance C, the electron mobility μ, and the electron attachment rate ν_a as constants, setting $\mu=0.06$ m^2/V s, $C=6\times10^{-12}$ F/m, and $\nu_a=7\times10^{-7}$ s^{-1}. Third, since the electron density n_e is still relatively low in this part of the discharge, we neglect recombination. The validity of these assumptions is discussed in Sec. IV and none of the assumptions are made in Sec. VII where we use the air chemistry code CHMAIR-II as the basis for complete numerical solutions of Eqs. (7) and (9a). Finally, we represent the continuing effect of photodetachment by replacing ν_a by the "net attachment" rate $\nu_a(1-n_{e0}/n_e)$, where n_{e0} is the electron density in the preionized channel, so that attachment does not cause n_e to drop below n_{e0} at the tip of the discharge.

With these assumptions, Eq. (7) can be rewritten as

$$\left(1+\frac{\mu E}{u}\right)\frac{1}{\Sigma}\frac{d\Sigma}{d\tau}+\frac{\mu}{u}\frac{dE}{d\tau}=\nu_i(E)-\nu_a\equiv\nu(E), \tag{10}$$

where we shall refer to ν as the net ionization rate. Swarm data[35] are usually presented in terms of the Townsend coefficient $\alpha_T\equiv\nu_i/\mu|E|$ and for air at atmospheric density we use the fit

$$\alpha_T=\begin{cases}5.78\times10^5e^{-1.90\times10^7/|E|}, & |E|<1.28\times10^7 \text{ V/m}\\ 1.11\times10^6e^{-2.73\times10^7/|E|}, & |E|>1.28\times10^7 \text{ V/m},\end{cases} \tag{11}$$

as shown in Fig. 2. Equations (9a) and (10) then constitute a self-contained pair of first-order ODEs for $E(\tau)$ and $\Sigma(\tau)$.

Note that the problem, as formulated in Eqs. (9a) and (10), depends on only two parameters, u and Σ_0, and on the

Downloaded 10 Feb 2011 to 132.250.22.10. Redistribution subject to AIP license or copyright; see http://pop.aip.org/about/rights_and_permissions

sign of E_0 which determines the polarity of the discharge. There is no dependence on either the channel radius $a(\tau)$ or on the radial profile of conductivity, since only the radially integrated conductance $\Sigma(\tau)$ appears in the 1D equations. However, the value of $a(\tau)$ does become important further back in the discharge where recombination and other processes begin to play a role.

Equations (9a) and (10) can be combined into a single self-contained expression for $E(\tau)$,

$$\frac{1}{E}\frac{dE}{d\tau} = \frac{Cu^2}{\Sigma_0}\left(1+\frac{\mu E}{u}\right)\exp\left[-\int_0^t d\tau' \frac{\nu(\tau')u - \mu dE/d\tau'}{u+\mu E(\tau')}\right] - \nu(\tau), \tag{12a}$$

which can also be written as an equation for the electron flow velocity $v(\tau)=-\mu E(\tau)$,

$$\frac{1}{v}\frac{dv}{d\tau} = \frac{Cu}{\Sigma_0}\left(\frac{u-v}{u}\right)\exp\left[-\int_0^\tau d\tau' \frac{\nu(\tau')u + dv/d\tau'}{u-v(\tau')}\right] - \nu(\tau). \tag{12b}$$

IV. STREAMER REGION: NEGATIVE DISCHARGE

In this section we consider discharges of negative polarity, $E_0<0$. We begin by showing that negative discharges must propagate at velocity

$$u > \mu E_b \approx 1.5\times 10^5 \text{ m/s}. \tag{13}$$

where E_b is the breakdown field in cold air. By definition, $\nu(E)=0$ at E_b.

At the tip of the discharge, ionization is negligible since $|E_0| \ll E_b$, attachment balances photodetachment, and $v=v_0=-\mu E_0 \ll u$. Thus $\nu=0$ and Eqs. (12) reduce to

$$E(\tau) \approx E_0 \exp(Cu^2\tau/\Sigma_0), \quad v(\tau) \approx v_0 \exp(Cu^2\tau/\Sigma_0). \tag{14}$$

In a negative discharge, $E(\tau)<0$ and $v(\tau)>0$. Since v is an increasing function of τ, $\nabla\cdot\mathbf{v}<0$ and the channel electrons bunch. Thus N_e and Σ increase with τ even though no ionization has occurred as yet. For $|E_0|<|E|<E_b$ and $n_e>n_{e0}$, ν is dominated by attachment and is negative. Therefore, as long as $v(\tau)<u$, both terms on the right-hand side (RHS) of Eq. (12b) are positive, and $v(\tau)$ continues to increase. But if Eq. (13) is not satisfied, $v(\tau)$ eventually exceeds u while $|E|<E_b$. At that point, the first term on the RHS of Eq. (12) becomes negative, and $v(\tau)$ can then continue to grow only if the net ionization rate $\nu(\tau)$ is negative. Accordingly $|E(\tau)|$ approaches E_b from below, gas breakdown does not occur, and there is no discharge.

This sequence of events is shown in Fig. 3 from a numerical solution of Eq. (12) for $C=6\times10^{-12}$ F/m, $\Sigma_0=10^{-9}$ m/Ω, $E_0=-10^4$ V/m, and $u=10^5$ m/s, which is below threshold (13). Although this solution is in the form of a traveling wave, it is sustained solely by electrons emitted from the cathode and cannot be regarded as a discharge since there is no breakdown.

In the remainder of this section, we consider cases where u is above threshold (13). In that case $|E(\tau)|$ eventually exceeds E_b and $\nu(\tau)$ turns positive. The field $E(\tau)$ and velocity $v(\tau)$ can then increase only as long as the first term on the RHS of Eq. (12) stays positive, and thus only as long as $v(\tau)<u$. Accordingly $v(\tau)$ never reaches u and $|E(\tau)|$ is bounded from above by u/μ. In Fig. 4, we show the solution of Eq. (12) for $C=6\times10^{-12}$ F/m, $\Sigma_0=10^{-9}$ m/Ω, $E_0=-10^4$ V/m, and $u=10^6$ m/s, which we shall regard as our baseline case. Initial exponential growth of $E(\tau)$ terminates once $|E|>E_b$, after which the last term of Eq. (12a) quickly becomes dominant as $\nu_i(E)$ increases rapidly from essentially zero to a value $\nu_i \gg \nu_a$. Thus, $|E(\tau)|$ overshoots E_b, but soon reaches a maximum, which we shall refer to as the E-spike, at a point $\tau=\tau_1$. If u is well above threshold (13), such that $\mu|E(\tau_1)| \ll u$; $E(\tau_1)$ is given approximately by the solution of $\nu[E(\tau_1)] \approx Cu^2/\Sigma_0$. After the spike, the RHS of Eq. (12) is negative, causing $|E(\tau)|$ to decrease. But $\nu(E)$

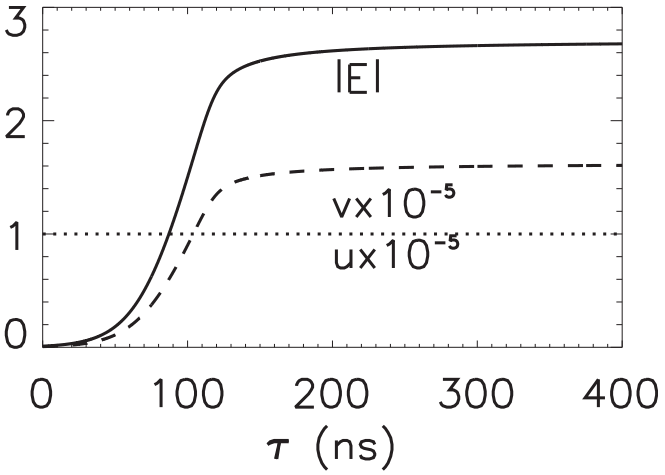

FIG. 3. $|E|(\tau)$ in units of MV/m (solid curve) and electron axial flow velocity $v(\tau)$ in units of 10^5 m/s (dashed curve) for negative polarity with $u=10^5$ m/s, below the threshold for breakdown.

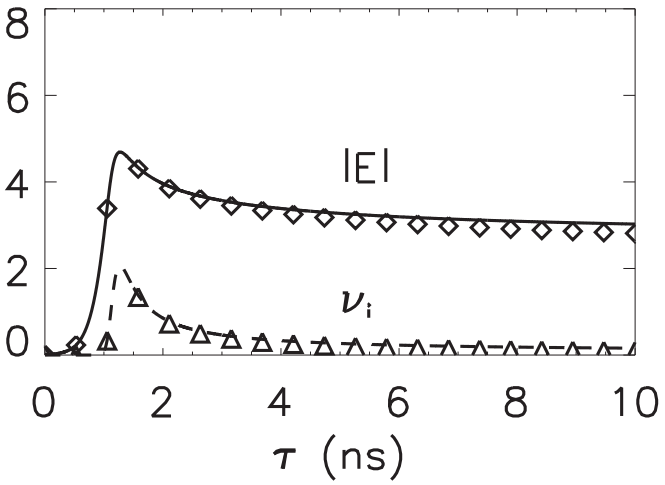

FIG. 4. $|E|(\tau)$ in units of MV/m (solid curve) and ionization rate $\nu_i(\tau)$ in units of 10^9 s^{-1} (dashed curve) for negative polarity with our baseline parameters ($a_0=2\times10^{-4}$ m, $\Sigma_0=10^{-9}$ m/Ω) and $u=10^6$ m/s. Diamonds and triangles: $|E|(\tau)$ and $\nu_i(\tau)$ from a simulation with attachment rate ν_a set to zero.

Downloaded 10 Feb 2011 to 132.250.22.10. Redistribution subject to AIP license or copyright; see http://pop.aip.org/about/rights_and_permissions

decreases even faster, and therefore the RHS of Eq. (12a) approaches zero. Thus,

$$\nu[E(\tau)] \to \frac{Cu^2}{\Sigma_0}\left[1+\frac{\mu E(\tau)}{u}\right] \times \exp\left\{-\int_0^\tau d\tau' \frac{\nu[E(\tau')]u-\mu dE/d\tau'}{u+\mu E(\tau')}\right\}. \quad (15)$$

The RHS of Eq. (15) is positive but steadily decreasing, and therefore the net ionization rate ν must be positive and steadily decreasing as well. Consequently,

$$|E| \to E_b \text{ from above.} \quad (16)$$

Thus, in the streamer region behind the E-spike, $E(\tau)$ is roughly constant at a value slightly more negative than $-E_b$, and the value of $E(\tau)$ is set, not by the electrodynamics, but by the requirement that there be some continuing net ionization so that $\Sigma(\tau)$ continues to increase.

Note two remarkable features of this analysis. First, one might think that a discharge can propagate with constant conductance $\Sigma(\tau)$ once breakdown has occurred. But in fact $\Sigma(\tau)$ must continue to increase. The underlying reason for this is that $E(\tau)<0$, so that $\phi(\tau)$ is negative and monotonically decreasing. Therefore the charge $C\phi(\tau)$ and current $I(\tau)=uC\phi(\tau)=\Sigma(\tau)E(\tau)$ are negative and monotonically decreasing functions of τ. But since $|E|$ is decreasing toward E_b, the current $|I(\tau)|$ can increase only if the conductance $\Sigma(\tau)$ grows. This remains true even during the leader phase discussed later and is a dominant feature of the physics. Second, we note that electron attachment has little effect on the nearly constant value of E, since the requirement that determines E is that $\nu_i-\nu_a$ be a small positive quantity (of order $1/\tau$), *not* that $\nu_i=\nu_a$. In the vicinity of E_b, $\nu_i(E)$ increases very rapidly from well below ν_a to well above ν_a. Thus, even if ν_a is set to zero (as it would be if the discharge was in nitrogen rather than air), the resulting solution, shown as the diamonds and triangles in Fig. 4, is nearly indistinguishable from the complete solution. These results additionally suggest that thermal detachment is unimportant and cannot account[36] for the streamer-leader transition, as argued by Gallimberti.[1]

To continue the analysis, we next obtain a rough estimate for the potential at the E-spike. Assuming that $E(\tau)$ is given approximately by Eq. (14) for $\tau<\tau_1$, we find that

$$\phi(\tau_1) = u\int_0^{\tau_1} d\tau E(\tau) \sim \text{order}(\Sigma_0 E_b/Cu), \quad (17)$$

which is typically a few kilovolts or less. Thus the potential drop from the E-spike to the tip of the discharge is small compared to the hundreds of kilovolts needed to drive long discharges. As a result, the breakdown region up to and including the E-spike has little influence on the overall energetics of the discharge, provided the propagation velocity threshold (13) is satisfied.

In the region behind the E-spike, $\Sigma(\tau)$ continues to increase while $E\approx -E_b$. The field remains clamped even as

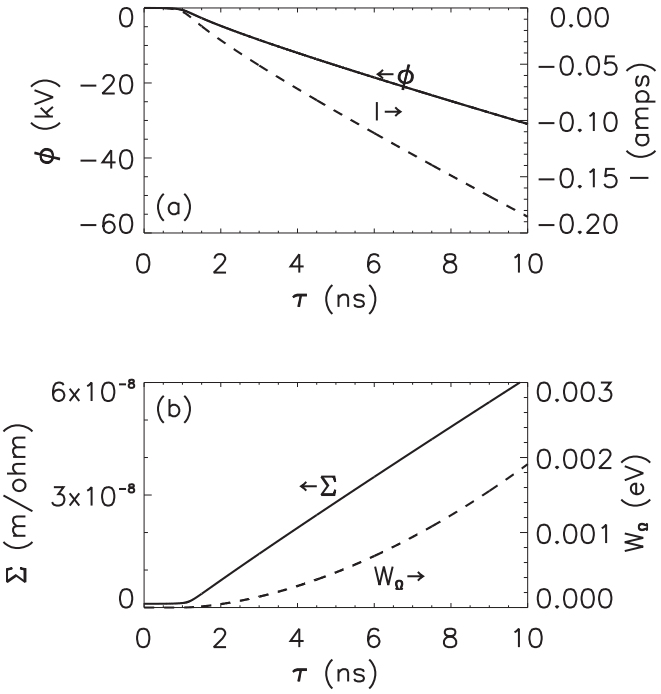

FIG. 5. (a) Potential $\phi(\tau)$ in kV (solid curve, left scale) and current $I(\tau)$ in amps (dashed curve, right scale), same simulation as Fig. 4. (b) Conductance Σ in m/Ω (solid curve, left scale), and Ohmic energy deposited per molecule W_Ω in eV (dashed curve, right scale).

processes like electron-ion recombination become important, because of the strong dependence of ν_i on E. Integrating $E(\tau)$ to get $\phi(\tau)$, we find that in this region

$$\phi(\tau) = u\int_0^\tau d\tau E(\tau) \approx \phi(\tau_1) - uE_b(\tau-\tau_1) \approx -uE_b\tau. \quad (18)$$

Thus, throughout the remainder of the streamer region, $|\phi(\tau)|$ increases nearly linearly with τ, as seen in Fig. 5(a).

In the early stages of propagation, the air is cool from the tip of the discharge at $\tau=0$ to the source at $\tau=t$. Hence the driving voltage pulse, for a discharge propagating at velocity u, must be $V(t)=\phi(\tau=t)\approx -uE_b(t-\tau_1)$. Turning the argument around, if we drive a discharge into a preionized channel by turning on a voltage pulse V(t), the discharge will propagate at speed $u\approx \dot{V}/E_b$, where $\dot{V}$ is the voltage rise rate in the early part of the pulse. This dependence has been observed experimentally.[37]

Another consequence of Eq. (16) is that the left hand side of Eq. (9d) goes to zero. Thus the conductance increases linearly with τ,

$$\Sigma(\tau) \approx \Sigma(\tau_1) + Cu^2(\tau-\tau_1) \quad \text{for} \quad \tau > \tau_1, \quad (19)$$

as seen in Fig. 5(b). Furthermore, inserting Eq. (19) into Eq. (10), we find that

Downloaded 10 Feb 2011 to 132.250.22.10. Redistribution subject to AIP license or copyright; see http://pop.aip.org/about/rights_and_permissions

$$\nu = \nu_i - \nu_a \rightarrow \left(1 + \frac{\mu E_b}{u}\right)\frac{Cu^2}{\Sigma(\tau_1) + Cu^2\tau} \rightarrow \left(1 + \frac{\mu E_b}{u}\right)\frac{1}{\tau}. \tag{20}$$

In pure nitrogen $\nu_a = 0$, but $\nu_i(E)$ is still a strong function of $|E|$. As a result, $|E|$ approaches a value only slightly less than E_b in air, which shows again that attachment has only a weak effect. Notice that most of the growth in Σ and ϕ occurs after the E-spike.

In the streamer region after the E-spike, the discharge current is

$$I(\tau) = E(\tau)\Sigma(\tau) \approx I(\tau_1) + CE_b u^2(\tau - \tau_1). \tag{21}$$

As with the potential $\phi(\tau)$ and the conductance $\Sigma(\tau)$, the current is small at the E-spike but then increases linearly with τ after the spike, as seen in Fig. 5(a). In this region $E(\tau)$, $\phi(\tau)$, $\Sigma(\tau)$, and $I(\tau)$ depend only on the single parameter u and not in any significant way on the initial conductance Σ_0. The influence of Σ_0 is felt only up to the E-spike.

The rate of Ohmic energy deposition is given by $IE = (d/d\tau)(C\phi^2/2) \approx CE_b^2u^2\tau$. Integrating over τ, we find that the total Ohmic energy deposited up to time τ, per air molecule, is

$$W_\Omega(\tau) \approx \frac{CE_b^2u^2\tau^2}{2\pi a_0^2 n_{g0}}. \tag{22}$$

Figure 5(b) shows a plot of $W_\Omega(\tau)$ for $a_0 = 2\times10^{-4}$ m. The Ohmic energy eventually heats the gas, and at that point the value of a_0 becomes important.

It is useful at this point in the discussion to consider the validity of some of our assumptions. The ionization rate ν_i depends on the electron velocity distribution, which in general depends on the *recent history* of the electric field $E(\tau)$. The Townsend ionization model,[3] however, assumes that ν_i depends on the *instantaneous* electric field, i.e., implicitly assumes that E has remained essentially constant over the time needed to establish a balance between Ohmic heating and electron energy losses, primarily to molecular vibrations and low-lying electronic excitations. This time scale is roughly 10^{-10} s for ambient air, short compared to the duration of the discharge (10^{-7} to 10^{-6} s), or even compared to the duration of the streamer stage, but it can be longer than the time scale Σ_0/Cu^2 for the growth of $E(\tau)$ in the breakdown region. In that case, the Townsend formula for ν_i is still roughly correct, but with $E(\tau)$ replaced by the back-average $\bar{E}(\tau) \equiv \int_{\tau-\Sigma_0/Cu^2}^{\tau}(Cu^2 d\tau'/\Sigma_0)E(\tau')$. This makes the E-spike somewhat higher and broader, but does not significantly affect our conclusions and has very little influence on the later evolution of the discharge. The Townsend assumption is thus generally sufficient, even for low Σ_0 or high u.

However, another of our assumptions comes into more serious question in the breakdown region where $\partial/\partial z$ is large. We pointed out in Eq. (1) that all transmission-line models assume $b(z,t)(\partial/\partial z) \ll 1$. This is well satisfied throughout most of the discharge, but in the breakdown region where $b(z,t) \approx a_0$ and $\partial/\partial z \sim Cu/\Sigma_0$, Eq. (1) reduces to

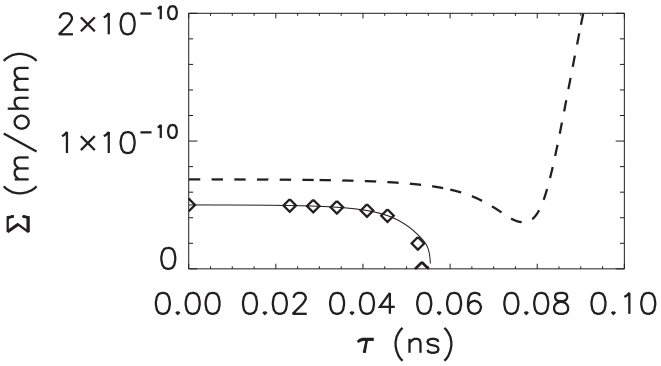

FIG. 6. Conductance $\Sigma(\tau)$ for positive polarity: below threshold case, $\Sigma_0 = 5\times10^{-11}$ m/Ω (solid curve); above-threshold case, $\Sigma_0 = 7\times10^{-11}$ m/Ω (dashed curve). Analytic solution (32) for the below-threshold case (diamonds).

$$\Sigma_0 > a_0 Cu. \tag{23}$$

If this assumption fails, as it does for a discharge into ambient air, multidimensional modeling is required, and the properties of the discharge may be fundamentally different. The differences between guided and unguided discharges are yet to be explored.

V. STREAMER REGION: POSITIVE DISCHARGE

In this section we show that discharges of positive polarity, $E_0 > 0$, can propagate only if the initial conductance Σ_0 exceeds another (stronger) threshold condition in addition to Eq. (23). We first combine Eqs. (9d) and (10) to obtain

$$\frac{d\Sigma}{d\tau} = \nu(E)\Sigma - Cu\mu E. \tag{24}$$

Initially $\nu = 0$ and $E = E_0 > 0$ for a positive discharge. Therefore $\Sigma(\tau)$ initially *decreases*, as electrons flow back toward the source with velocity $v(\tau) < 0$. Meanwhile $E(\tau)$ grows exponentially according to Eq. (14), eventually exceeding E_b, at which point ν increases very rapidly. Thus two types of evolution are possible: either (1) $\Sigma(\tau)$ reaches a minimum and then increases, leading to a viable discharge, or (2) $\Sigma(\tau)$ decreases to zero at finite time, in which case there is no discharge. These two behaviors are illustrated in Fig. 6, which was obtained by solving Eqs. (12) for $u = 10^6$ m/s, $E_0 = +10^4$ V/m, and $C = 6\times10^{-12}$ F/m. For the solid curve, the initial conductance was so small, $\Sigma_0 = 5\times10^{-11}$ m/Ω, that $\Sigma(\tau)$ reached zero. There was no discharge. The dashed curve shows a case initiated with a slightly higher conductance, $\Sigma_0 = 7\times10^{-11}$ m/Ω. In this case, $\Sigma(\tau)$ reached a minimum and rebounded, and a discharge did occur.

To determine the threshold needed for Σ_0, assume that $\Sigma(\tau)$ decreases until reaching a minimum at time τ_{min}. According to Eq. (24),

$$\Sigma(\tau_{min}) = \frac{Cu\mu E(\tau_{min})}{\nu[E(\tau_{min})]} \approx \frac{Cu}{\alpha_T(\tau_{min})}, \tag{25}$$

where in the last term we have assumed that $\nu[E(\tau_{min})] \approx \nu_i[E(\tau_{min})] \gg \nu_a$. This is justified in air provided $E(\tau_{min}) \geq 1.3E_b$. A discharge occurs only if there is a solution for

Downloaded 10 Feb 2011 to 132.250.22.10. Redistribution subject to AIP license or copyright; see http://pop.aip.org/about/rights_and_permissions

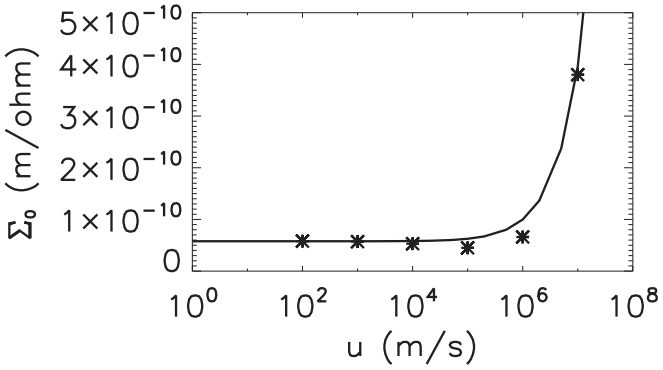

FIG. 7. Threshold channel preconductivity Σ_0 for propagation of a positive discharge: solid curve from analytic theory, Eqs. (29) and (30); asterisks are from the numerical solution of Eq. (12).

τ_{min}. For $\tau < \tau_{min}$, the RHS of Eq. (7) is essentially zero, and thus initially

$$\Sigma(\tau) \approx \frac{u + \mu E_0}{u + \mu E(\tau)} \Sigma_0 \approx \frac{u \Sigma_0}{u + \mu E(\tau)}. \tag{26}$$

Equation (26) is quite accurate from $\tau = 0$ nearly up to $\tau = \tau_{min}$. We can therefore combine Eqs. (25) and (26) to obtain

$$\Sigma_0 \approx \frac{u + \mu E(\tau_{min})}{\alpha_T [E(\tau_{min})]} C. \tag{27}$$

$\Sigma(\tau)$ reaches a minimum and begins to grow if and only if there is a value of E which satisfies Eq. (27). As shown in Fig. 2, α_T increases rapidly with E when E is small but slowly when E is large. The right-hand side of Eq. (27) therefore has a minimum at some value $E = \tilde{E}$, such that

$$\left. \frac{d \ln(\alpha_T)}{dE} \right|_{E=\tilde{E}} = \frac{\mu}{u + \mu \tilde{E}}. \tag{28}$$

Hence, positive discharges can propagate only if

$$\Sigma_0 \geq \frac{C(u + \mu \tilde{E})}{(\alpha_T \tilde{E})}. \tag{29}$$

Using the form $\alpha_T(E) \propto \exp(-B/E)$ from Eqs. (11), we find

$$\tilde{E} = \frac{B}{2} + \sqrt{\left(\frac{B}{2}\right)^2 + \frac{uB}{\mu}}. \tag{30}$$

Equations (29) and (30) thus define the threshold Σ_0 as a function of u, which is plotted in Fig. 7 (solid curve). Figure 7 also shows the threshold found from full numerical solutions of Eqs. (12a) for various values of u and Σ_0. The analytic calculation shows excellent agreement with the numerical solutions.

To further elucidate the evolution of $\Sigma(\tau)$, we use Eq. (26) to eliminate E from Eq. (9d), thereby producing a closed ODE for $\Sigma(\tau)$,

$$\frac{d\Sigma}{d\tau} = Cu^2 - \frac{Cu(u + \mu E_0)\Sigma(\tau)}{\Sigma_0}, \tag{31}$$

valid for $\tau < \tau_{min}$. Integrating this equation produces

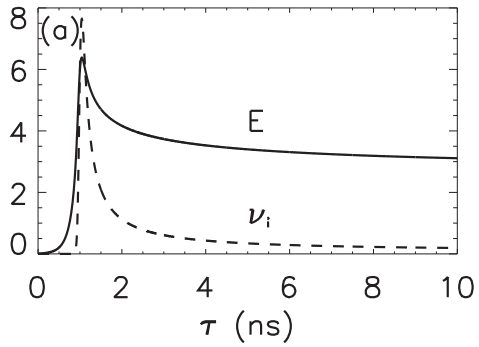

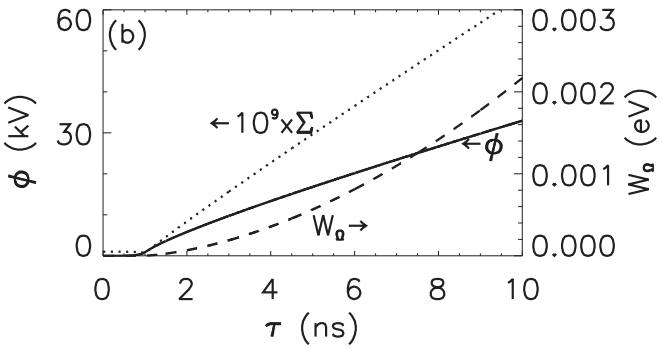

FIG. 8. Positive discharge with the same parameters as the negative discharge of Fig. 4. (a) $E(\tau)$ in MV/m (solid curve) and ionization rate $\nu_i(\tau)$ in units of 10^9 s^{-1} (dashed curve). (b) $\phi(\tau)$ in kV (solid curve, left scale), Σ in units of 10^{-9} m/Ω (dotted curve, left scale) and W_Ω in eV (dashed curve, right scale)

$$\frac{Cu^2 \tau}{\Sigma_0} = \left(\frac{\Sigma - \Sigma_0}{\Sigma_0}\right) + \left(1 + \frac{\mu E_0}{u}\right) \ln\left[1 + \left(\frac{u}{\mu E_0}\right)\left(\frac{\Sigma - \Sigma_0}{\Sigma_0}\right)\right]. \tag{32}$$

The diamonds in Fig. 6 show solution (32) for the below-threshold case cited above with $\Sigma_0 = 5 \times 10^{-11}$ m/Ω. Note that $\Sigma(\tau)$ goes to zero at a finite time $\tau \approx 0.044$ ns. The full numerical solution of Eq. (12) (solid curve) shows very nearly the same behavior.

If Σ_0 exceeds threshold (29), $E(\tau)$ overshoots E_b and rises sharply to a peak just past τ_{min}, as seen in Fig. 8. The last term in Eq. (9d) is then dominant and causes $E(\tau)$ to collapse. Comparing Fig. 8 to Figs. 4 and 5, we see that the subsequent evolution is very similar to that of the negative discharge, with $|E(\tau)|$ again approaching and clamping at E_b, as required by Eq. (16). Similarly, $\phi(\tau)$, $\Sigma(\tau)$, and $I(\tau)$ all soon increase linearly with τ according to Eqs. (18), (19), and (21). Indeed, positive and negative discharges have almost identical structure when $u \gg \mu |E(\tau_1)|$, since Σ is then controlled almost entirely by the balance of ionization and deionization rather than by axial electron flow. In both cases, the value of Σ_0 has little influence on the discharge after the E-spike.

VI. HEATED AIR CHANNEL: BASIC CONSIDERATIONS

A fundamental conclusion of the previous sections is that if the discharge is to propagate at a constant velocity, the

Downloaded 10 Feb 2011 to 132.250.22.10. Redistribution subject to AIP license or copyright; see http://pop.aip.org/about/rights_and_permissions

conductance $\Sigma(\tau)$ must increase on a timescale that is comparable to the value of τ itself. Thus $\nu_i - \nu_a$ must be positive but small. In cold ambient air, this requires that $|E| \approx E_b \approx 2.7$ MV/m. If this condition held throughout the pulse, a 1 MV discharge could propagate no farther than 0.4 m.

However, the more general requirement is that the RHS of Eq. (7) be positive. This requires ionization, since detachment merely offsets attachment and does not produce any net growth in Σ. The electron ionization rate ν_i is determined by the electron energy distribution, which is roughly characterized by the electron temperature T_e. Thus for most of the discharge, breakdown is possible only if T_e equals or exceeds a threshold T_b, where T_b is the temperature at which ν_i equals the total electron loss rate. Typically $T_b \approx 1.8$ eV in both air and nitrogen, since attachment has only a weak effect. This condition on T_e holds until the gas becomes highly dissociated, at which point associative ionization ($N+O \rightarrow NO^+ + e$) becomes important and T_e slowly decreases. But until then E needs to be sufficiently large for Ohmic heating to maintain T_e just above T_b. We shall now show that a laser-guided discharge, propagating within a sufficiently narrow conducting channel, can heat the air so that a single streamer (cold air discharge) grows into a leader (hot air discharge).

The value of E in the main body of the discharge ultimately determines how far a discharge can propagate for given voltage V(t). As discussed above, E is determined as the field necessary to maintain $T_e \approx T_b$, until the gas becomes highly dissociated. The requirement in cold air is $|E| \approx E_b$, but much lower values are sufficient once the air becomes hot and excited. Propagation to ranges $\gg 0.4$ m/MV is thus possible, as seen experimentally.[4–17] T_e is related to E through a static balance between Ohmic heating and electron cooling,

$$\Sigma E^2 = N_e Q_c, \tag{33}$$

where Q_c is the net electron cooling rate due to gas excitation, dissociation, ionization, etc. Included in Q_c are superelastic collisions, which feed energy stored in vibrational and electronic excitation back to the electrons. Although Q_c is complicated and depends on the state of the gas, several key features of Q_c can be identified.

Early in time T_e is high (~ 2 eV) while the temperatures characterizing the other degrees of freedom of the plasma are close to the ambient temperature, $T_0 \approx 0.025$ eV. During this time the major electron cooling mechanism is vibrational excitation of the nitrogen molecule, and to model this process we treat the nitrogen molecule as a harmonic oscillator[38] with vibrational temperature T_v. As energy goes into the vibrational modes, T_v increases, eventually approaching T_e. Vibrational energy then flows back to the electrons, and Q_c and E begin to decrease. The decrease in E due to saturation of the vibrational modes becomes noticeable in CHMAIR-II once T_v rises above 0.15 eV, a prediction consistent with more complete Boltzmann calculations.[39] At that point the plasma energy content is $W(\tau) \approx 0.08$ eV/molecule, split roughly equally between N_2 vibrational modes and electronic excitation[40] of the N_2 and O_2 molecules. We identify this as the time τ_2 for the onset of vibrational heating.

As $W(\tau)$ continues to increase, a sequence of events ensues which ultimately drives the plasma toward local thermodynamic equilibrium (LTE): first the low-lying electronic states begin to be heavily populated, then the higher-lying states are excited, followed by dissociation, the formation of new molecular species, and an increase in the heavy-particle kinetic temperature T_g. If LTE is reached, all plasma parameters, including the temperature T (which then characterizes all degrees of freedom), the dissociation fraction, and the free electron density n_e, become functions mainly of $W(\tau)$.[41,42] Channel expansion, radiation, and thermal conduction/convection become the major cooling mechanisms, and $W(\tau)$ falls below $W_\Omega(\tau)$ as energy flows out of the channel. As we shall see, channel expansion in particular results in a substantial further decrease in E. These effects become noticeable when $W(\tau) \approx 0.3$ eV/molecule, and we shall identify this as the time τ_3 for the onset of gas heating.

Since $W(\tau) \approx W_\Omega(\tau)$ for $\tau \leq \tau_3$, the times τ_2 and τ_3 can be estimated by time-integrating the Ohmic heating rate per unit length, ΣE^2. This has already been done analytically in Eq. (22) and the results are shown in Figs. 5 and 8. For example, using Eq. (22), we estimate that gas heating begins at time τ_3 such that

$$\frac{C E_b^{\,2} u^2 \tau_3^{\,2}}{2\pi a_0^{\,2} n_{g0}} \approx 0.3 \text{ eV} \approx 5 \times 10^{-20} \text{ J}, \tag{34a}$$

or equivalently the distance behind the head of the discharge is given (in mks units) by

$$u\tau_3 \approx \frac{2800 a_0}{C^{1/2} E_b}. \tag{34b}$$

According to Eq. (18) the potential at this point is

$$\phi(\tau_3) = 2900 C^{-1/2} a_0. \tag{35}$$

Note that the onset of gas heating depends crucially on the energy deposited per air molecule, and therefore on the number of air molecules per unit length, $\pi a_0^2 n_{g0}$, contained in the channel. Thus the initial channel radius a_0, which was irrelevant in the streamer region, becomes a critical parameter in the leader. On the other hand, neither $u\tau_3$ (the distance from the discharge tip to the point where gas heating begins) nor $\phi(\tau_3)$ depends on the speed u. For $C = 17 \times 10^{-12}$ F [a typical value at this point in the discharge, where $b(\tau)$ is of the order of several centimeters] and $a_0 = 200$ μm, gas heating begins once the discharge has propagated $u\tau_3 \approx 6$ cm, at which point $V(t) \geq 160$ kV. A single streamer can therefore transition into a leader as long as the applied voltage is sufficiently high, over 160 kV in the present example, and only then is long range possible. Since $\phi(\tau_3)$ scales proportionally to a_0, the driving voltage must be higher if a_0 exceeds 200 μm.

Once the channel becomes hot, it expands so as to maintain pressure balance with the ambient air. The time scale for expansion is $\sim a/c_s$, where $a(\tau)$ is the channel radius and c_s is the sound speed in the channel. The propagation time is L/u, and thus there is ample time for expansion to occur as long as $a_0 \ll (c_s/u)L$. Expansion does not change the number of electrons per unit length, but it does dissipate some of the energy deposited in the channel through PdV work per-

Downloaded 10 Feb 2011 to 132.250.22.10. Redistribution subject to AIP license or copyright; see http://pop.aip.org/about/rights_and_permissions

formed on the surrounding air, thereby decreasing the rate at which the gas temperature T_g rises. Furthermore, expansion substantially increases the electron mobility, since the density of electron scatterers (mainly molecules) is reduced inversely to a^2. Expansion thus increases the conductance $\Sigma(\tau) \equiv eN_e\mu$, which further increases the range of the discharge.

VII. CHMAIR-II SIMULATIONS

As outlined above, the leader phase is complicated and involves many processes. Our computational tool for modeling these processes is the CHMAIR-II code,[13,34] and in the studies presented here, ambient air was assumed to consist of nitrogen and oxygen molecules in 4:1 ratio. The version of CHMAIR-II employed in these studies uses over 100 reactions to follow the time evolution of the densities of N_2, N, O_2, O, NO, N^+, N_2^+, N_3^+, N_4^+, O^+, O_2^+, O_4^+, NO^+, O^-, and O_2^-, as well as the densities of several key metastables. Charge balance is used to determine the source and sink rates for the electron density n_e, and energy equations are used to separately determine the electron temperature $T_e(\tau)$, the gas temperature $T_g(\tau)$, and the nitrogen vibrational temperature $T_v(\tau)$. Electron ionization, attachment, recombination, detachment, and mobility are included through T_e-dependent coefficients, obtained by integrating the relevant cross sections over a Maxwellian electron energy distribution[43] at temperature T_e. These coefficients, and those for all other key processes, agree well with those published elsewhere.[38,44] We emphasize that the objective of this work is not to calculate all of the discharge properties in quantitative detail, but rather to understand the general physics and scaling laws governing discharge propagation.

For initial conditions, we typically assume $T_e=0.5$ eV and $T_g=T_v=0.025$ eV. Photodetachment is represented by the mock-up described in Sec. III, and the discharge is assumed to propagate at specified constant speed u so that all quantities are functions of the single variable τ as before. The axial electric field E is calculated from Eq. (9a). The discharge is assumed to be uniform within radius $a(\tau)$, with a(0) set to the specified channel radius a_0. After each time step, the plasma is allowed to expand radially to keep the channel at atmospheric pressure P_0. Loss of plasma internal energy to PdV work is included self-consistently, with P set equal to P_0. However, if the radial expansion rate $\dot{a}$ is found to exceed the sound speed c_s of the heated channel, then $\dot{a}$ is limited to c_s, the pressure is calculated self-consistently and is allowed to temporarily exceed P_0, and the actual channel pressure P is used in calculating the PdV work. As a check, the LTE conductivity σ_{LTE} is calculated from $W(\tau)$, and the code includes the option to switch to σ_{LTE} if it exceeds the conductivity σ_{CHM} calculated from the rate equations. This may be necessary in future studies, since CHMAIR-II does not impose detailed balance, treats air as optically thin, and does not include all of the reactions and states that play a role in the LTE regime. In these studies we find that σ_{LTE} is never much larger than σ_{CHM}, and the two values are similar when the gas is hot, $T_g > 0.5$ eV.

In this section we present the results of several CHMAIR-II simulations and discuss scaling with the independent parameters of our model, i.e., the discharge speed u, preexisting channel conductivity Σ_0, and initial discharge radius a_0. We begin by examining the transition from the cool-air "streamer" regime, which was studied in Secs. III–V with the Townsend breakdown model, to the hot gas "leader" regime. Figure 9 (solid curve) shows the CHMAIR result for the electric field $E(\tau)$ in the range $0 \le \tau \le 100$ ns, for a negative discharge with our baseline parameters from Fig. 4: $u = 10^6$ m/s, $a_0 = 2 \times 10^{-4}$ m, and $\Sigma_0 = 10^{-9}$ m/Ω. Notice that $|E| > E_b$ up to $\tau \approx 40$ ns, but that $|E|$ falls well below E_b at later times, reaching 2.1 MV/m, and continuing to decrease rapidly at $\tau = 100$ ns. For comparison, the dashed curve shows $E(\tau)$ from a CHMAIR run wherein T_v and T_g were frozen at room temperature, and the dotted curve shows $E(\tau)$ from the Townsend model (an extension of Fig. 4). The latter two results are similar,[43] with E approaching a constant in each case, as discussed in Sec. IV Clearly, the heating of the vibrational modes is responsible[39] for the drop-off in E, which leads to range extension, and the onset time for significant vibrational heating in this run is $\tau_2 \approx 40$ ns. That time marks the beginning of the transition to the leader phase.

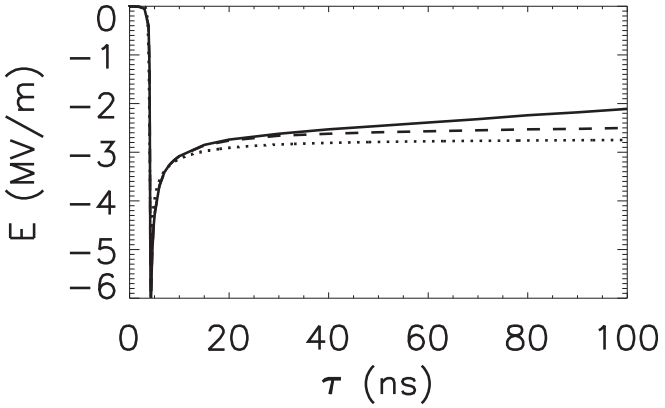

FIG. 9. CHMAIR-II result (solid curve) for $E(\tau)$ for a negative discharge with the parameters of Fig. 4. CHMAIR-II calculation (dashed curve) with T_v and T_g frozen at room temperature. The same calculation done with the Townsend model (dotted curve).

Figure 10 shows $T_e(\tau)$, $T_v(\tau)$, $T_g(\tau)$, and the Ohmic energy deposition $W_\Omega(\tau)$. At $\tau = \tau_2$, T_g is still quite cold but $T_v \approx 0.15$ eV, still well below T_e but substantially above room temperature T_0. At this time $W_\Omega \approx 0.08$ eV. Figures 9 and 10, taken together, are in good quantitative agreement with the discussion of Sec. VI. Notice that $T_e(\tau) \approx 2.2$ eV is very slowly decreasing and slightly above $T_b \approx 1.8$ eV. We show in addition, as the diamonds in Fig. 10, $T_e(\tau)$ from the CHMAIR-II run (dashed curve of Fig. 9) with T_v frozen at T_0. We see that the presence or absence of vibrational heating significantly affects E but has no discernable effect on $T_e(\tau)$. This is an illustration of the underlying principle that T_e is clamped at a value slightly above T_b to keep the conductance growing, and E adjusts to maintain T_e at this value. Notice also that T_g begins to rise at time $\tau_3 \approx 80$ ns when $W_\Omega \approx 0.3$ eV, in agreement with the discussion of Sec. VI The

Downloaded 10 Feb 2011 to 132.250.22.10. Redistribution subject to AIP license or copyright; see http://pop.aip.org/about/rights_and_permissions

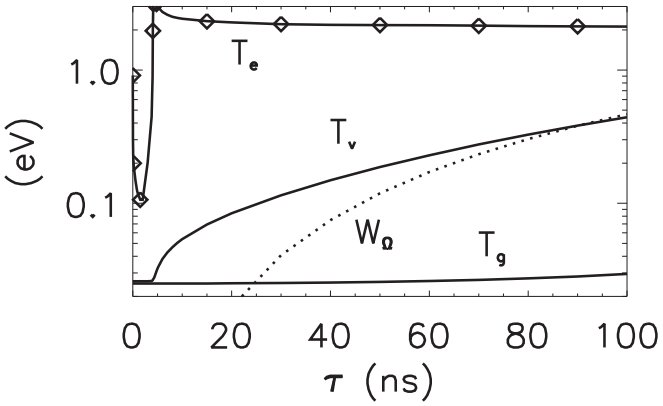

FIG. 10. CHMAIR-II results for $T_e(\tau)$, $T_v(\tau)$, $T_g(\tau)$ (solid curves), and $W_\Omega(\tau)$ (dotted curve) for the simulation (solid curve) in Fig. 9. $T_e(\tau)$ from a CHMAIR-II simulation with T_v and T_g frozen (diamonds).

value of τ_3 is in reasonable agreement with the estimate of 60 ns from Eq. (34b).

Figure 11 shows $E(\tau)$ for three different cases: the base-line case (negative discharge of Fig. 9, solid curve), a positive discharge with the same parameters (dashed curve), and a negative discharge with the same parameters except that Σ_0, the conductance of the preionized channel, is reduced by an order of magnitude to 10^{-10} m/Ω (dotted curve). The only visible difference between the positive and negative discharges is that the E-spike is somewhat higher for the positive case, for reasons discussed in Sec. V The two cases are virtually identical after the E-spike and will have the same range, carry the same current, etc. Similarly, in the dotted case the time scale for the initial exponential growth of $E(\tau)$ is reduced proportionally to the smaller Σ_0, as discussed in Sec. V, but after the E-spike the result is nearly identical. These results demonstrate that the polarity of the discharge and the value of Σ_0 significantly affect the breakdown region but not the main body of the discharge. For long discharges, the breakdown region sets threshold conditions for propagation, as discussed in Secs. IV and V, but dissipates little energy, is responsible for only a small fraction of the ionization, and carries a small potential drop. The parameters that

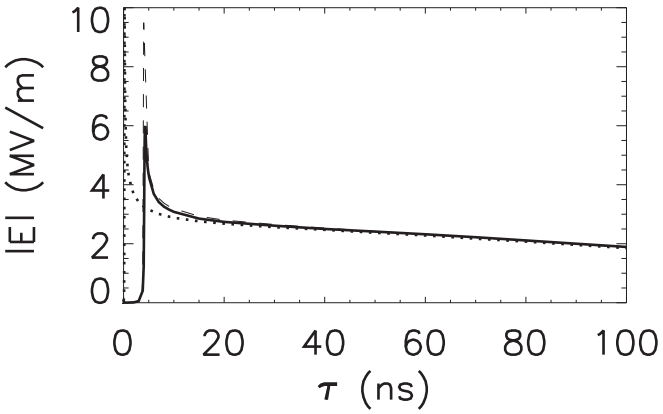

FIG. 11. CHMAIR-II results for $E(\tau)$ for the negative discharge of Fig. 9 (solid curve), positive discharge with the same parameters (dashed curve), and negative discharge with the same parameters except that Σ_0 is reduced by an order of magnitude to 10^{-10} m/Ω (dotted curve).

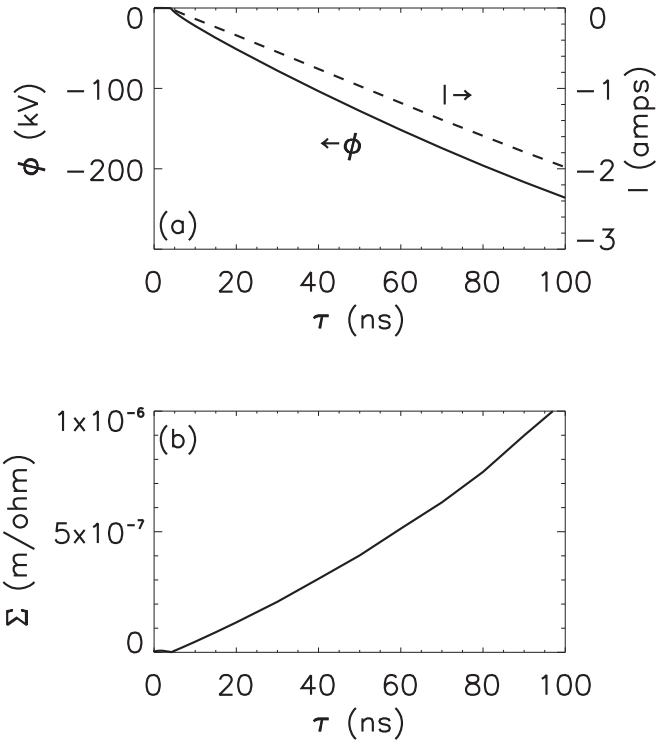

FIG. 12. (a) CHMAIR-II results for the negative discharge of Fig. 9: (a) $\phi(\tau)$ (solid curve, left scale) and current $I(\tau)$ (dashed curve, right scale), and (b) $\Sigma(\tau)$.

control the discharge body are the discharge speed u and the initial radius a_0.

Figure 12 shows $I(\tau)$, $\Sigma(\tau)$, and $\phi(\tau)$ for the baseline negative discharge. Notice that all three quantities begin to increase linearly with τ after the E-spike at $\tau=9$ ns, as in Fig. 5, but as $T_v(\tau)$ increases and the transition to the leader begins, $|\dot{\phi}(\tau)|$ rolls off while $\dot{\Sigma}(\tau)$ increases.

Figure 13 shows the effect of channel expansion at late time on $|E(\tau)|$, $\Sigma(\tau)$, $T_g(\tau)$, and the discharge radius $a(\tau)$ for the base-line example shown in Fig. 12. The solid curves include thermal expansion as described in Sec. VI, while the dashed curves have thermal expansion turned off. The two sets of curves begin to separate noticeably at $\tau \approx 80$ ns when $T_g \approx 1.1T_0$, and we see that channel expansion substantially increases the conductance, as discussed in Sec. VI, thereby decreasing $E(\tau)$ and greatly increasing the range. Channel expansion also substantially delays the increase in T_g (due to the energy expended in PdV work on the surrounding gas), which alters the late time chemistry in many ways.

In Fig. 14, we show $E(\tau)$, $I(\tau)$, $\phi(\tau)$, $\Sigma(\tau)$, and $T_e(\tau)$ for a complete negative discharge with our baseline parameters ($a_0=200$ μm, $u=10^6$ m/s), propagating to $\tau=2$ μs and range $u\tau=2$ m. About 25% of the voltage drop occurs in the cold gas region prior to $\tau_3 \approx 80$ ns, and another 25% early in the leader region ($\tau<200$ ns) before channel expansion has fully kicked in. Thereafter, E steadily falls and is quite small at the end of the run, so that a small increase in driving voltage equates to a substantial increase in range (as long as conditions are such that the discharge continues to follow the laser filament). The current $I(\tau)$ increases throughout the discharge, but slowly in the leader stage as required by Eq. (9b).

Downloaded 10 Feb 2011 to 132.250.22.10. Redistribution subject to AIP license or copyright; see http://pop.aip.org/about/rights_and_permissions

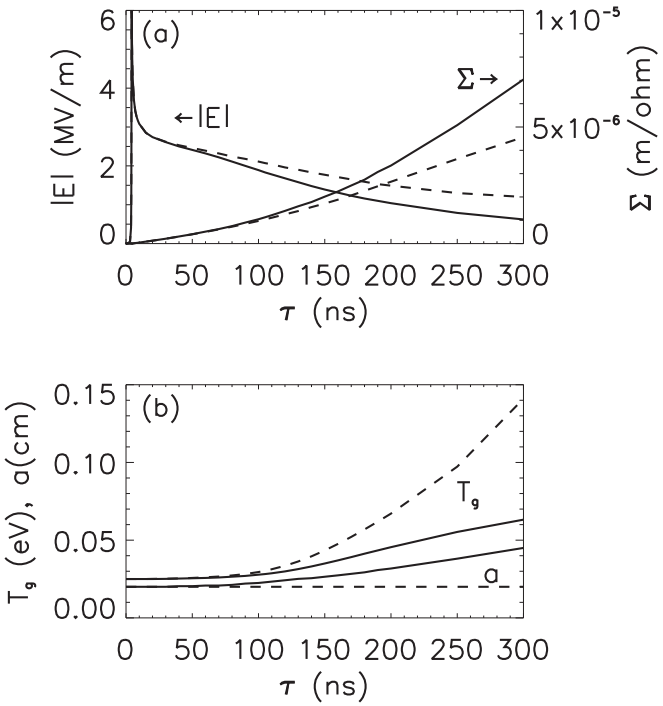

FIG. 13. CHMAIR-II results for the negative discharge of Fig. 9: (a) $|E(\tau)|$ (left scale) and $\Sigma(\tau)$ (right scale) (b) $T_g(\tau)$ and $a(\tau)$. Solid curves include expansion, dashed curves do not.

The conductance $\Sigma(\tau)$ also increases throughout the discharge. To sustain the steady increase in $\Sigma(\tau)$, T_e remains clamped near $T_b=1.8$ eV throughout most of the discharge, even as all the other parameters are varying strongly.[45] However, the chemical composition of the gas changes throughout the discharge, and the degree of excitation increases, eventually making it easier to ionize the gas and leading to a drop in T_e and a surge in $\Sigma(\tau)$ toward the end of the run.

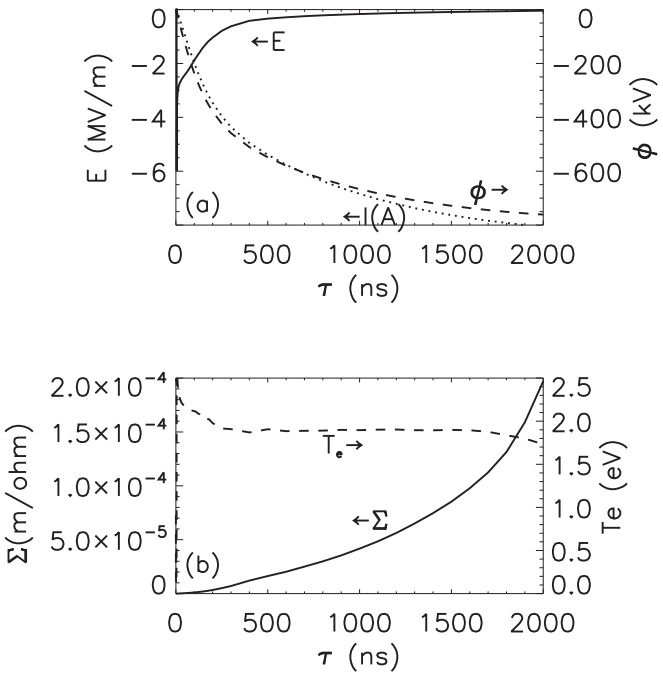

FIG. 14. CHMAIR-II results for the negative discharge of Fig. 9: (a) $E(\tau)$ (solid curve, left scale), $I(\tau)$ (dotted curve, left scale), $\phi(\tau)$ (dashed curve, right scale); (b) $\Sigma(\tau)$ (solid curve, left scale) and $T_e(\tau)$ (dashed curve, right scale).

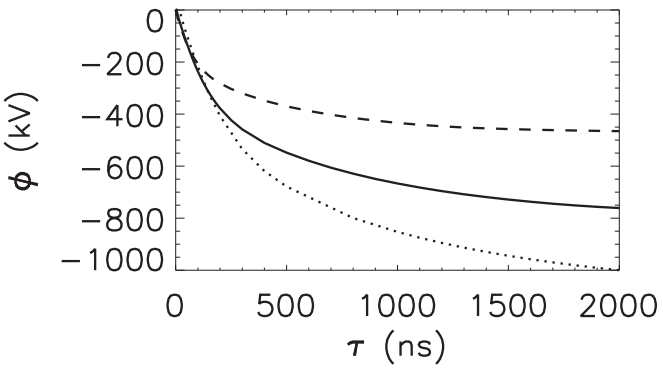

FIG. 15. Potential $\phi(\tau)$ for the negative discharge of Fig. 9: $a_0=200$ μm (solid curve), $a_0=100$ μm (dashed curve), and $a_0=300$ μm (dotted curve).

In Fig. 15, we show $\phi(\tau)$ for our baseline case but with three different initial radii: $a_0=200$ μm (solid curve), $a_0=100$ μm (dashed curve), and $a_0=300$ μm (dotted curve). For any given driving voltage, range is seen to increase rapidly as a_0 is decreased. The number of molecules contained in the discharge scales as a_0^2, and when the energy dissipated in the channel is spread among fewer molecules, vibrational excitation, gas heating, and channel expansion all occur earlier. All of these factors increase $\Sigma(\tau)$, thereby decreasing $E(\tau)$ and increasing the range.

We next consider the scaling with discharge velocity u. Figure 16 shows the evolution of a negative discharge with our baseline parameters, except that u is increased to 10^7 m/s. This is to be compared with Fig. 14, where $u=10^6$ m/s. We consider first the relationship between the driving voltage V(t) and the value of u. As discussed in Sec. IV, we found that in the streamer regime u is propor-

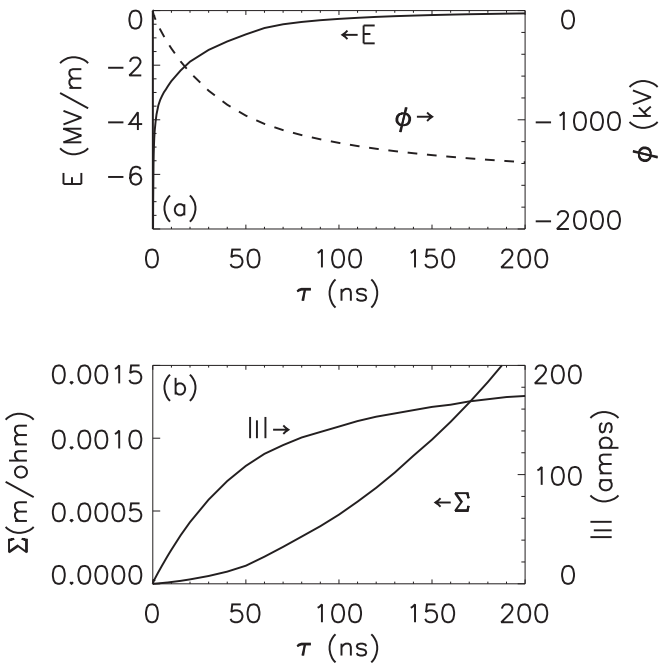

FIG. 16. CHMAIR-II results for a case with the parameters of Fig. 9, except $u=10^7$ m/s instead of 10^6 m/s: (a) $E(\tau)$ (solid curve, left scale) and $\phi(\tau)$ in kV (dashed curve, right scale); (b) $\Sigma(\tau)$ (left scale) and $|I(\tau)|$ (right scale).

Downloaded 10 Feb 2011 to 132.250.22.10. Redistribution subject to AIP license or copyright; see http://pop.aip.org/about/rights_and_permissions

tional to the rise rate of V(t). We have not found any similar relation for the leader regime, but comparing Figs. 14 and 16, we see that the voltage rise rate dV/dt is still an increasing function of u. Rephrasing this statement in terms of the experimentally controllable quantity V(t), a rapid voltage rise results in a fast propagation speed u. Finally, we consider the dependence of the propagation range on u. Again comparing $\phi(\tau)$ from Figs. 15 and 16, and noting that the propagation distance is $L=u\tau$, it is apparent that for any given driving voltage V, the propagation range is a decreasing function of u. For example, at driving voltage 760 kV, the range is 2 m when $u=10^6$ m/s (Fig. 14) but only 30 cm when $u=10^7$ m/s (Fig. 16). Stated differently, for a given maximum driving voltage V, range is a *decreasing* function of the voltage rise rate. Our model is strictly applicable only when the propagation speed u is constant, but it is reasonable to infer that in general the range increases strongly as a function of the maximum voltage, but decreases as a function of the voltage rise rate.

VIII. CONCLUSIONS

We have presented a 1D model for laser-guided discharges, based on two primary sets of assumptions: (1) reduction of the 3D electrodynamic/conductivity evolution equations to 1D time-dependent transmission-line form, based on the assumptions that the discharge propagates within a specified uniform conductivity channel, and that axial variations are slow compared to the radial spatial scales; and (2) reduction of these equations to ordinary differential equations in retarded time, based on the assumption that the discharge propagation speed is constant. We have then used both analytic techniques and numerical solutions to sketch out the consequences of the model. The model depends on three parameters, the propagation speed u, the pre-existing conductance of the laser channel Σ_0, and the initial discharge radius a_0, and it also depends on the positive or negative polarity of the discharge.

We find that the discharge can be divided into a streamer region (at the front), wherein the electrons are hot but all other degrees of freedom of the gas are cold, a transition region, wherein molecular vibrations and low-lying electronic states are excited, but the molecular thermal energy is low, and a leader region, wherein the gas is hot and highly excited.

In the streamer region, the ionization rate $\nu_i(\tau)$ is a function only of the instantaneous electric field $E(\tau)$. Initially $E(\tau)$ increases exponentially at rate Cu^2/Σ_0. In this region, there are significant differences between positive and negative discharges, because the divergence of the axial electron flow can significantly affect the time evolution of the electron density. One consequence is that negative discharges can propagate only at propagation speeds $u > E_b/\mu$. Positive streamers, on the other hand, can propagate at speeds below E_b/μ but require a preconductance Σ_0 in excess of a threshold value $\Sigma_{thr}(u)$ to advance; the threshold is plotted in Fig. 7 and is roughly equal to 6×10^{-11} m/Ω for $u<10^6$ m/s. Exponential growth of $E(\tau)$ terminates at a peak of the electric field, the "E-spike." Thereafter E decreases and remains roughly constant at the breakdown field E_b, and the conductance $\Sigma(\tau)$, current $I(\tau)$, and potential $\phi(\tau)$ all increase nearly linearly in τ. The energy deposited via Ohmic heating thus increases as τ^2, and during this period typically little energy is lost from the channel by radiation or thermal conduction/convection.

However, one of the basic assumptions of the model, slow variation in z, holds in the initial breakdown stage at the tip of the discharge only if $\Sigma_0 > a_0 Cu$, Eq. (23). This suggests that Eq. (23) constitutes a threshold condition for guided discharges of the type seen in this paper, with a single fast streamer following a prepared cylindrical channel and growing into a leader. With no preionization, or with Σ_0 below threshold, the physics may be quite different, leading to the 2D or 3D type of initial streamer breakdown, typically with smaller propagation speed u, which is seen experimentally in discharges into ambient gas. The observed differences between guided and unguided discharges are discussed by Pepin *et al.*[9] Further exploration of this suggested threshold condition is a compelling subject for future work.

When the Ohmic energy deposited reaches ~0.15 eV/molecule, the discharge enters the transition stage wherein the excitation of vibrations and low-lying electronic states begin to play a role. Once the gas is excited, the Townsend relation no longer holds, and it is more appropriate to think of ν_i as a function of the electron temperature T_e, rather than a function of E. The electron density continues to increase, and thus ν_i must slightly exceed the attachment and recombination rates. This requirement determines the value of T_e, which remains nearly constant throughout the remainder of the discharge, and $|E(\tau)|$ takes the value necessary to maintain T_e at this level. As the degree of excitation increases, $|E|$ falls well below E_b, thereby enabling propagation of the discharge to extended range for a given applied voltage.

Eventually the discharge enters the leader stage where the gas molecules are hot, partially dissociated, and highly excited. The chemistry becomes more complicated and the hot channel expands to maintain pressure balance. The conductance increases proportionally to a^2, which leads to a nearly proportionate decrease in E and subsequent increase in the propagation range.

We find that the range of long discharges is insensitive to the initial conductance Σ_0, except that Σ_0 must exceed $a_0 Cu$ for the model to be valid and exceed Σ_{thr} for positive discharges to propagate. However, the range depends strongly on both the initial radius a_0 and the propagation speed u. Decreasing a_0 leads to a large increase in range, because the number of molecules contained within the discharge is proportional to a_0^2, so the mean energy per molecule increases if a_0 is reduced. Therefore the discharge enters the leader stage earlier, expands earlier, and becomes hotter and more highly conducting. This dependence on a_0 could also explain why laser-guided discharges usually propagate to greater range (as compared to unguided discharges) for a given driving voltage.[9] Unguided discharges are believed to advance via multiple streamers which coalesce to form a single leader, whose radius is then determined by breakdown processes and turns out to be relatively large.[3] Laser-guided discharges,

Downloaded 10 Feb 2011 to 132.250.22.10. Redistribution subject to AIP license or copyright; see http://pop.aip.org/about/rights_and_permissions

on the other hand, generally advance along a single laser-produced plasma filament, and the leader radius is determined by the filament radius (as well as by subsequent recombination and ionization processes), and is normally quite narrow.

Finally, we have found that the range, for any given driving voltage, is a decreasing function of the propagation speed u. Since u is an increasing function of the voltage rise rate, it follows that for any given maximum driving voltage, the range will be larger if the voltage pulse V(t) ultimately rises slowly.

ACKNOWLEDGMENTS

This work was supported by the Office of Naval Research and by the Army Research Office, Development and Engineering Center. The authors are grateful to Dr. Phillip Sprangle for originating and encouraging this research and for contributing to the initial stages of the work.. The authors also extend special thanks to Dr. A. Wahab Ali, the guiding spirit behind the CHMAIR-II code.

[1] I. Gallimberti, J. Phys. Colloq. **40**, C7-193 (1979); A. Bondiou and I. Gallimberti, J. Phys. D **27**, 1252 (1994).
[2] Yu. P. Raizer, *Gas Discharge Physics* (Springer, New York, 1997).
[3] E. M. Bazelyan and Yu. P. Raizer, *Spark Discharge* (CRC, Boca Raton, 1998).
[4] M. Miki and A. Wada, J. Appl. Phys. **80**, 3208 (1996).
[5] B. La Fontaine, F. Vidal, D. Comtois, C. Y. Chien, A. Desparois, T. W. Johnston, J. C. Kieffer, H. P. Mercure, H. Pépin, and F. A. M. Rizk, IEEE Trans. Plasma Sci. **27**, 688 (1999).
[6] B. La Fontaine, D. Comtois, C.-Y. Chien, A. Desparois, F. Génin, G. Jarry, T. Johnston, J.-C. Kieffer, F. Martin, R. Mawassi, H. Pépin, F. A. M. Rizk, F. Vidal, C. Potvin, P. Couture, and H. P. Mercure, J. Appl. Phys. **88**, 610 (2000).
[7] D. Comtois, C. Y. Chien, A. Desparois, F. Génin, G. Jarry, T. W. Johnston, J.-C. Kieffer, B. La Fontaine, F. Martin, R. Mawassi, H. Pépin, F. A. M. Rizk, F. Vidal, P. Couture, H. P. Mercure, C. Potvin, A. Bondiou-Clergerie, and I. Gallimberti, Appl. Phys. Lett. **76**, 819 (2000).
[8] A. Desparois, B. La Fontaine, A. Bondiou-Clergerie, C.-Y. Chien, D. Comtois, T. Johnston, J.-C. Kieffer, H. P. Mercure, H. Pepin, F. A. M. Rizk, and F. Vidal, IEEE Trans. Plasma Sci. **28**, 1755 (2000).
[9] H. Pépin, D. Comtois, F. Vidal, C. Y. Chien, A. Desparois, T. W. Johnston, J. C. Kieffer, B. La Fontaine, F. Martin, F. A. M. Rizk, C. Potvin, P. Couture, H. P. Mercure, A. Bondiou-Clergerie, P. Lalande, and I. Gallimberti, Phys. Plasmas **8**, 2532 (2001).
[10] M. Rodriguez, R. Sauerbrey, H. Wille, L. Wöste, T. Fujii, Y.-B. André, A. Mysyrowicz, L. Klingbeil, K. Rethmeier, W. Kalkner, J. Kasparian, E. Salmon, J. Yu, and J.-P. Wolf, Opt. Lett. **27**, 772 (2002).
[11] D. Comtois, H. Pepin, F. Vidal, F. A. M. Rizk, C.-Y. Chien, T. W. Johnston, J.-C. Kieffer, B. La Fontaine, F. Martin, C. Potvin, P. Couture, H. P. Mercure, A. Bondiou-Clergerie, P. Lalande, and I. Gallimberti, IEEE Trans. Plasma Sci. **31**, 377 (2003).
[12] P. Baronavski, H. D. Ladouceur, and P. G. Giradi, "Experimental observations of electrical arc discharges along laser-induced plasma channels," NRL Memorandum Report No. NRL/MR/6110-02-8642, 2002.
[13] D. F. Gordon, A. Ting, R. F. Hubbard, E. Briscoe, C. Manka, S. P. Slinker, A. P. Baronavski, H. D. Ladouceur, P. W. Grounds, and P. G. Girardi, Phys. Plasmas **10**, 4530 (2003).
[14] R. Ackermann, K. Stelmaszczyk, P. Rohwetter, G. Méjean, E. Salmon, J. Yu, J. Kasparian, G. Méchain, V. Bergmann, S. Schaper, B. Weise, T. Kumm, K. Rethmeier, W. Kalkner, L. Wöste, and J. P. Wolf, Appl. Phys. Lett. **85**, 5781 (2004).
[15] R. Ackermann, G. Méchain, G. Méjean, R. Bourayou, M. Rodriguez, K. Stelmaszczyk, J. Kasparian, J. Yu, E. Salmon, S. Tzortzaki, Y.-B. André, J.-F. Bourrillon, L. Tamin, J.-P. Cascelli, C. Campo, C. Davoise, A. Mysyrowicz, R. Sauerbrey, L. Wöste, and J.-P. Wolf., Appl. Phys. B: Lasers Opt. **82**, 561 (2006).
[16] X. M. Zhao, J.-C. Diels, C. Y. Wang, and J. M. Elizondo, IEEE J. Quantum Electron. **31**, 599 (1995).
[17] J. Kasparian, R. Ackermann, Y.-B. André, G. Méchain, G. Méjean, B. Prade, P. Rohwetter, E. Salmon, K. Stelmaszczyk, J. Yu, A. Mysyrowicz, R. Sauerbrey, L. Woeste, and J.-P. Wolf, Opt. Express **16**, 5757 (2008).
[18] H. Schillinger and R. Sauerbrey, Appl. Phys. B: Lasers Opt. **68**, 753 (1989).
[19] D. C. Gary, G. Le Roy, B. Hutzler, J. Lalot, and C. Dubanton, *Collection Direction des Etudes et Rechereches d'Electricite de France* (Editions Eyrolles, Paris, 1984), Chap. 17, p. 22.
[20] J. Sasaki, S. Kubodera, R. Ozaki, and T. Uchiyama, J. Appl. Phys. **60**, 3845 (1986).
[21] G. E. Georghiou, R. Morrow, and A. C. Metaxas, J. Phys. D **32**, 1370 (1999).
[22] N. Y. Babaeva and G. W. Naidis, IEEE Trans. Plasma Sci. **25**, 375 (1997).
[23] A. A. Kulikovsky, J. Phys. D **30**, 441 (1997); **30**, 1515 (1997); **33**, 1514 (2000).
[24] M. M. Nudnova and A. Yu. Starikovskii, J. Phys. D **41**, 234003 (2008).
[25] A. P. Papadakis, G. E. Georghiou, and A. C. Metaxas, J. Phys. D **41**, 234019 (2008).
[26] F. Vidal, D. Comtois, C.-Y. Chien, A. Desparois, B. La Fontaine, T. W. Johnston, J.-C. Kieffer, H. P. Mercure, H. Pepin, and F. A. M. Rizk, IEEE Trans. Plasma Sci. **28**, 418 (2000).
[27] N. Y. Aleksandrov, A. E. Bazelyan, E. M. Bazelyan, and I. V. Kochetov, Plasma Phys. Rep. **21**, 57 (1995).
[28] N. Y. Aleksandrov and E. M. Bazelyan, Plasma Phys. Rep. **27**, 1057 (2001).
[29] D. Comtois, H. Pepin, F. Vidal, F. A. M. Rizk, C.-Y. Chien, T. W. Johnston, J.-C. Kieffer, B. La Fontaine, F. Martin, C. Potvin, P. Couture, H. P. Mercure, A. Bondiou-Clergerie, P. Lalande, and I. Gallimberti, IEEE Trans. Plasma Sci. **31**, 387 (2003).
[30] N. L. Aleksandrov, É. M. Bazelian, N. A. Bogatov, A. M. Kiselev, and A. N. Stepanov, Plasma Phys. Rep. **34**, 1059 (2008).
[31] R. F. Fernsler, NRL Memorandum Report No. 5026, 1983, available from the National Technical Information Service as Document No. ADA126286, may be accessed at the NTIS homepage http://www.NTIS.gov; A related 2D (r–z) model was discussed in R. F. Fernsler, Phys. Fluids **27**, 1005 (1984).
[32] J. K. Wright, Proc. R. Soc. London, Ser. A **280**, 23 (1964).
[33] E. Marode, J. Appl. Phys. **46**, 2005 (1975).
[34] R. F. Fernsler, A. W. Ali, J. R. Greig, and I. M. Vitkovitsky, NRL Memorandum Report No. 110, 1979. Available as EPAPS suppplementary material E-PHPAEN-10-049311, may be accessed at EPAPS homepage http://www.aip.org/pubservs/epaps.html or from ftp.aip.org in the directory /epaps/.
[35] J. Dutton, J. Phys. Chem. Ref. Data **4**, 577 (1975).
[36] N. L. Aleksandrov and E. M. Bazelyan, Plasma Sources Sci. Technol. **8**, 285 (1999).
[37] G. J. J. Winands, Z. Liu, A. J. M. Pemen, E. J. M. van Heesch, and K. Yan, J. Phys. D **41**, 234001 (2008).
[38] M. Capitelli, C. M. Ferreira, B. F. Gordiets, and A. I. Osipov, *Plasma Kinetics in Atmospheric Gases* (Springer, Berlin, 2000).
[39] G. Colonna, M. Capitelli, C. Morse, F. Panicca, A. V. Eletski, and B. M. Smirnov, Nuovo Cimento **14**, 585 (1992).
[40] A. W. Ali, "Electron energy loss rates in N_2, O_2 and air," NRL Memorandum Report No. NRL-MR-5400, 1984.
[41] F. Burhorne and R. Wienecke, Z. Phys. Chem. **215**, 269 (1960).
[42] A. D'Angola, G. Colonna, C. Gorse, and M. Capitelli, Eur. J. Phys. **D46**, 129 (2008).
[43] The assumption of a Maxwellian distribution to calculate the ionization coefficient $\nu_i(E)$ leads to a calculated value of E_b that is 15% lower than the experimental value of 2.5 MV/m. To correct this inaccuracy, in CHMAIR-II we multiply the Maxwellian value for $\nu_i(T_e)$ by 0.45, which resets E_b to 2.5MV/m. This modification has only a slight effect on $E(\tau)$ and $\phi(\tau)$. The streamer model described in Sec. III overestimates E_b by roughly 8%, leading to a small disagreement between the two models.
[44] I. A. Kossyi, A. Y. Kostinsky, A. A. Matveyev, and V. P. Silakov, Plasma Sources Sci. Technol. **1**, 207 (1992).
[45] In the regime relevant to these calculations, electron scattering is due primarily to electron-molecule collisions. Thus conductivity is proportional to n_e, and T_e must be large enough to produce positive net ionization. If n_e becomes large enough so that mobility is limited by electron-ion collisions, we enter the regime of Spitzer conductivity, which is insensitive to n_e but scales as $\sigma \sim T_e^{3/2}$.

Downloaded 10 Feb 2011 to 132.250.22.10. Redistribution subject to AIP license or copyright; see http://pop.aip.org/about/rights_and_permissions